Compensation of Shallow Donors by Gallium Vacancies in Monoclinic β-Ga_2O_3

Santosh K. Swain, Marc H. Weber, Jani Jesenovec, Muad Saleh, Kelvin G. Lynn,[†] and John S. McCloy[*]

Institute for Materials Research, Washington State University, Pullman, Washington 99164, USA

(Received 24 July 2020; revised 10 February 2021; accepted 21 April 2021; published 5 May 2021)

Knowledge of the origin of deep levels and their impact on electrical properties is critical for device applications of β-Ga_2O_3. By annealing under an oxygen (O_2) atmosphere, the resistivity in shallow-donor (zirconium) doped β-Ga_2O_3:Zr single crystals is found to increase by more than 10 orders of magnitude to $(7 \pm 4) \times 10^{10}$ Ω cm, which is comparable to the resistivity achieved by iron (Fe) acceptor doping of $(5 \pm 3) \times 10^{11}$ Ω cm. We combine thermoelectric effect spectroscopy and positron annihilation spectroscopy (PAS), which are sensitive to deep levels and concentration of open-volume defects, with modeling of the electrical properties, to study these strongly compensated crystals. We find the compensating level in the O_2-annealed β-Ga_2O_3:Zr sample to be located at (0.727 ± 0.021) eV ($E2^*$) below the conduction band, which correlates with a vacancy signal from PAS data. The defect is most likely the relaxed split Ga vacancy V_{Ga}^{i}, rather than a simple gallium vacancy, considering theoretical predictions of a small energy barrier to relax. We observe that, due to the unique nature of these vacancies and anisotropy in the monoclinic lattice, the Doppler-broadening parameter is rather small compared with other wide-gap compounds, and in such a case the positron diffusion length is a suitable parameter to estimate the open-volume defect concentration.

DOI: 10.1103/PhysRevApplied.15.054010

I. INTRODUCTION

Ultrawide-band-gap β-Ga_2O_3 is emerging as the material of choice for next-generation power electronics suitable for high-voltage and high-frequency operations, UV detectors, high-temperature gas sensors, and potential nanophotonic devices due to its attractive properties, including a large band gap of about 4.8 eV, high breakdown field of about 8 MV/cm, low on-state resistance, and availability of low-defect-density native substrates both highly *n*-type and semi-insulating [1–8]. Similar to many other wide-gap oxides, high *p*-type conductivity is challenging to obtain, due to the localized oxygen *p* orbital, and hole self-trapping [9]. High *n*-type conductivity is typically obtained by doping with Si, Sn, or Ge [10]. Recently, we demonstrated a similar or higher electron concentration with zirconium (Zr) or hafnium (Hf) doping, with additional advantages of higher mobility, higher dopant solubility, and lower dopant vapor pressure [11,12].

Acceptors in β-Ga_2O_3 are deep, and these defects can influence the electrical and optical properties as compensation and recombination centers. Deep extrinsic acceptors Fe and Mg are known to cause high resistivity and are used to obtain semi-insulating wafers by various melt growth techniques. Here, we report that high resistivity, comparable to that obtained by deep acceptor doping, is achieved by annealing shallow-donor-doped crystals under an oxygen (O_2) atmosphere and creating a sufficient concentration of native defects. Among the possible native defects, the formation of gallium vacancies (V_{Ga}) and associated defect complexes with hydrogen are thermodynamically favorable under oxygen-rich conditions for Fermi-level positions closer to the conduction band, and they are predicted to be deep acceptors [13–15]. Techniques such as electron paramagnetic resonance and infrared spectroscopy studies identify these defects [16–18]. Positron annihilation studies show a high concentration of open-volume defects related to V_{Ga} under oxygen-rich conditions, which causes compensation of Si donors [19,20]. Deep acceptors with various energy levels are reported to reduce the *n*-type conductivity in donor-doped and undoped β-Ga_2O_3 films and bulk crystals [21–24].

The techniques that are commonly employed to determine the energy levels and defect concentrations, based on capacitance transients, generally use conductive samples with free-electron concentrations of about 10^{16} cm^{-3} or higher, but these measurements are challenging when the material becomes semi-insulating. Furthermore, the presence of an electric field during emission from the traps is reported to alter the estimated trap parameters due to field-enhanced emission rates [25]. To quantitatively describe electrical compensation in shallow-donor-doped

[*]john.mccloy@wsu.edu
[†]Deceased.

β-Ga_2O_3 and identify the origin of the involved defect, we apply thermoelectric effect spectroscopy (TEES), which is sensitive to deep levels in semi-insulating materials, and positron annihilation spectroscopy (PAS), with its sensitivity to vacancy-type defects in neutral and negatively charged states [26,27].

II. EXPERIMENTAL METHODS

A. Thermoelectric effect spectroscopy

In this study, two types of bulk single crystals are investigated by TEES. One is a zirconium-doped crystal (β-Ga_2O_3:Zr), with a room-temperature electron concentration of about 5×10^{17} cm^{-3}, that was cleaved in (100) orientation from a Czochralski- (CZ) grown boule. The growth and electrical properties are described elsewhere [11]. The crystal is annealed at 1050 or 1400 °C for 15 h under an oxygen atmosphere. The second sample is a CZ-grown Fe-doped crystal provided by Northrup Grumman Synoptics. The orientation for the Fe-doped sample is not measured, but believed to be either (100) or (001), as it is easy to cleave layers from the sample surface. TEES measurement involves trap filling at a low temperature by optical excitation followed by thermal emission from the trap during heating. In TEES, the driving force to extract thermally emitted carriers is a temperature gradient, rather than a bias across the thickness of the sample. The technique works best for materials with low thermal conductivity and is particularly suitable for high-resistivity materials, where the dark current is low enough to allow observation of a current signal from traps, which is typically in the order of a few picoamps (pA). TEES has been applied in the past to semi-insulating GaAs [28], GaN [29], Cd-Zn-Te [30], and CdTe [31], to identify native defects, dopants, and complexes. The energy level of the traps can be extracted from the initial onset of the current or by applying different heating rates in multiple scans, i.e., the variable-heating-rate (VHR) method. The VHR method commonly used in conductivity glow curve analysis [32] is used to estimate the trap energies and cross section using

$$\ln\left(\frac{T_M^2}{\beta}\right) = \frac{E_{\rm th}}{k_B T_M} - \ln\left(\frac{\sigma_{\rm th} v_n N_c k_B}{E_{\rm th}}\right). \qquad (1)$$

$E_{\rm th}$ is the thermal ionization energy, T_M is the temperature corresponding to maximum current, β is the heating rate with units K/s, k_B is the Boltzmann constant, $\sigma_{\rm th}$ is the trapping cross section, v_n is the carrier thermal velocity, and N_c is the effective density of states.

Samples for TEES measurements have an area of about 8×8 mm^2 and thickness of (1–2) mm. Planar contacts of Ga + In are applied on the top and bottom surfaces of the sample and are connected to a Keithley 6517 electrometer for current measurements. The samples are illuminated with subband-gap photons (365, 385, or 400 nm), for 1000 s at a low temperature. TEES spectra are collected by heating the sample at constant rates between 0.05 and 0.3 K/s, with an imposed temperature gradient of 10 K across the thickness.

B. Positron annihilation spectroscopy

Samples for PAS include, in addition to the two samples studied by TEES, an undoped crystal grown using high-purity Ga_2O_3 powder, labeled as HP; an unintentionally doped (UID) sample in the as-grown not-annealed state (UID-na) and following annealing in O_2 at 1050 or 1400 °C; and a Zr-doped sample annealed at 1400 °C. We employ Doppler-broadened PAS, with a monoenergetic variable-energy positron beam up to 70 keV, equivalent to a mean implantation depth of about 6.3 μm in β-Ga_2O_3. After implantation in the sample, the positron thermalizes in a few picoseconds, followed by thermal diffusion and possible trapping at open-volume defects, if present, in neutral or negatively charged states, leading to an increase in annihilations with low-momentum delocalized electrons. Doppler broadening is measured with a pair of high-purity germanium (HPGe) detectors with an energy resolution of 1.45 keV full width at half maximum at 511 keV and a high detection efficiency of >100% relative to NaI scintillators. The second detector is used in coincidence to counteract positrons that backscatter from the sample and annihilate near but not on the sample, a systematic effect that cannot be ignored for materials with a high average atomic number (Z) and high density, such as Ga_2O_3.

The Doppler-broadening signal is composed of annihilation events in a narrow central 1.5-keV-wide window of the 511 keV annihilation peak, the S parameter, and a partially anticorrelated signal from the wings of the peak, the W parameter, 2.6 to 5.85 keV from the peak. S and W are normalized by the total peak rate in a 11.7-keV window after background subtraction. When positrons trap in vacancies prior to annihilation, the central S fraction increases, and the W fraction decreases with increasing concentration in vacancies. In contrast, the peak is broadened for annihilations in a defect-free lattice, where the positron annihilates from its delocalized bulk state, carrying contributions from high-momentum core electrons. W also contains annihilations with high-momentum electrons bound to atoms next to the vacancy. This adds a defect-type specific component to W. A linear correlation of S versus W with a constant slope indicates changes in the concentration of a single defect type. Changes in slope point to changes in the defect type. The dynamic range is determined by the bulk S value (S_b) for a defect-free lattice and the S value for saturation trapping (S_d) when all positrons annihilate from a trapped state. The dynamic range typically spans about 6 orders of magnitude in defect concentration. However, the technique is most sensitive to

defect concentration (c_d) in the range of about 1×10^{16} to 5×10^{18} cm^{-3}. The vacancy defect concentration, c_d, is estimated using

$$c_d = \frac{N}{\mu\tau}\frac{S - S_b}{S_d - S}. \quad (2)$$

N is the number density of atoms, 3.78×10^{22} cm^{-3}, for Ga_2O_3; μ is a specific trapping rate of about 3×10^{15}/s [27,33] for negatively charged vacancies; and τ is the positron lifetime in the defect-free lattice, for which a value of 176 ps is used [19]. Like in many other crystalline materials, particularly when they are more complex than basic semiconductors, such as silicon and germanium, a perfect defect-free reference sample is not available. The estimation of a defect concentration remains that, an estimate. A crystal grown at WSU from high-purity starting material, however, shows evidence of high quality from a positron perspective. A bulk lifetime measurement is consistent with a single lifetime of 176 ps. A longer component, in the order of 400 ps, with an intensity of several percent, is likely due to the ^{22}Na source deposited directly onto the sample. 176 ps is consistent with the lifetime reported by Ting *et al.* [34]. VEPFit of depth profile data in the [001] orientation yields a good fit with a single layer, $S_{\text{layer}} = 0.4160 \pm 0.0003$, and a diffusion length of $L = (92 \pm 8)$ nm.

Unlike more commonly studied semiconductors, the electronic structure of β-Ga_2O_3 is highly anisotropic [35]. The Doppler signature is found to change, depending on the direction of emitted annihilation photons relative to the lattice orientation. Second, the gallium vacancy (V_{Ga}), which can exist at tetrahedral and octahedral sites, is also found to relax into a split configuration, where a gallium atom sits on an interstitial site between two gallium vacancies, V^i_{Ga}, of which three configurations are possible, due to the low energy barrier of about 0.53 eV to relax into the split state [36]. Karjalainen *et al.* [35] have shown that this leads to an unusually small vacancy Doppler signal, S, of only about 2 to 3% above defect-free Ga_2O_3. The values are used in lieu of a perfect sample. The Doppler value of $S = 0.4160$ for the [001] orientation is the lowest and the result for the [010] orientation is about 2% higher, which is consistent with the work reported in Ref. [35].

The defect concentration, c_d, can also be estimated from the measured positron diffusion length, L, which is another defect-sensitive parameter in PAS. In defect-free material, it reflects the finite lifetime of positrons. Depth profiles of positron annihilations can be used to extract the positron diffusion length. The observed depth profile is a convolution of the actual damage depth profile with the implantation profile and the diffusion of thermal positrons until trapping or annihilation from the defect-free state. The diffusion length decreases from L_b (bulk value) to L_d (saturation trapping) with increasing concentration of trapping defects, c_d, which can be estimated using

$$c_d = \frac{N}{\mu\tau}\left(\frac{L_b^2}{L_d^2} - 1\right). \quad (3)$$

The values obtained from the high-purity source-material sample are used to estimate the defect concentration (c_d), assuming, $S_b = 0.4160$, $S_d \sim 1.03 S_b$, and a diffusion length of $L_b = 100$ nm ≥ 92 nm in the same sample. The resulting defect concentrations should be considered as lower limits based on the uncertainty about the "defect-free" nature of the reference sample.

Theoretical work on β-Ga_2O_3 predicts a positron wave function aligned as near-one-dimensional channels along the [001] axis along tubes of large open spaces in the crystal lattice and perpendicular to the main cleavage plane. Implanting positrons in this direction and detecting the Doppler signal in the two perpendicular directions yields the lowest and highest S as a function of orientation. The diffusion of positrons, however, is independent of this quasirotation of the detector around the sample. Diffusion or tunneling of positrons perpendicular to this direction is possible. The diffusion length, L, has a larger dynamic range than the relatively small range in S of 2%–3%. L may be a better measure of the defect concentration in Ga_2O_3.

III. RESULTS AND DISCUSSION

A. Electrically compensating acceptor levels observed in TEES

Following oxygen annealing, the resistivity of the β-Ga_2O_3:Zr sample increases by nearly 10 orders of magnitude from about 0.1 Ω cm to 7×10^{10} Ω cm, whereas the as-grown Fe-doped sample has a resistivity of $(5 \pm 3) \times 10^{11}$ Ω cm. The current versus voltage (I-V) characteristics of these samples are shown in Fig. 1.

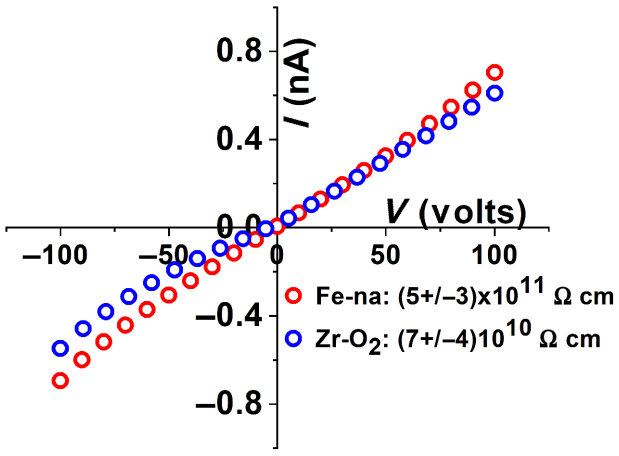

FIG. 1. I-V characteristics of O_2-annealed Zr-doped sample and Fe-doped not annealed (Fe-na) crystal.

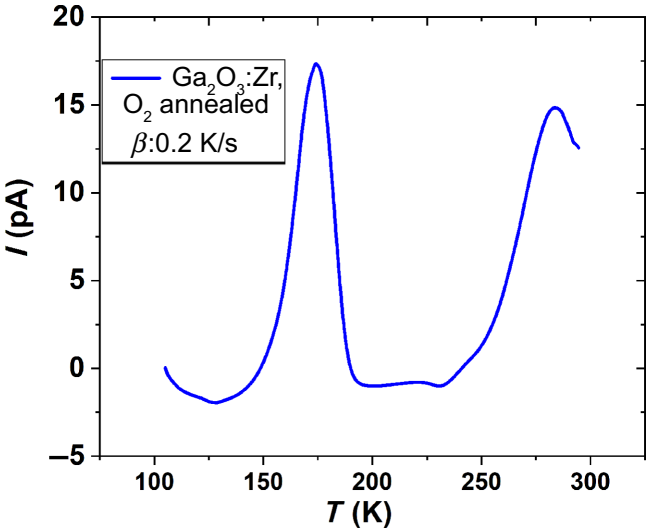

FIG. 2. TEES spectrum of O_2-annealed β-Ga_2O_3:Zr sample, obtained at a heating rate of 0.2 K/s, and illumination with 365 nm at 100 K.

High resistivity in Fe-doped crystals is known to be caused by Fe acceptors located (0.75–0.82) eV below the conduction band [37,38]. Here, we investigate the origin of high resistivity in O_2-annealed β-Ga_2O_3:Zr. Two prominent defect levels (TEES current peaks) at about 175 and 280 K are observed in the TEES spectrum for this sample, as shown in Fig. 2.

Arrhenius fits using Eq. (1) estimate energies of (0.573 ± 0.030) and (0.727 ± 0.021) eV, respectively, for traps observed near 175 and 280 K. Deep electron traps with similar energies are reported in various β-Ga_2O_3 single crystals and films; however, their origins are not clearly determined [24,39,40].

The VHR method used here to estimate the trap energy assumes negligible retrapping of emitted carriers. In cases when recombination is not monomolecular, the VHR method can give erroneous values for trap parameters. We also apply the initial rise method, which disregards any recombination kinetics, since very early in the trap-emptying process, far from the temperature corresponding to maximum TEES current (T_M), the emission is thermally activated. However, the technique is sensitive to the selection of the initial current. Therefore, to avoid distortions in the current baseline, trap filling is performed at a temperature (180 K) where the lower-temperature traps are left empty. Figures 3(a) and 3(b) show the energy of the trap near 280 K determined by the VHR method $[(0.727 \pm 0.021)$ eV] and the initial rise method $[(0.734 \pm 0.008)$ eV], confirming the accuracy of the estimated energy.

Here, to quantitatively describe compensation in the O_2-annealed β-Ga_2O_3:Zr, sample, we model the resistivity, taking into account the observed traps at 0.573 and 0.73 eV and the measured values for donor concentration, N_D (5×10^{17} cm^{-3}), and energy level, E_D (15 meV), before annealing [11]. Using charge neutrality, we obtain the resistivity as a function of concentration of deep acceptors (N_A) with energies (E_A) at about 0.573 eV and about 0.73 eV below the conduction band, as follows:

$$p + \frac{N_D}{1 + g_D\, e^{(E_F - E_D)/kT}} = n + \frac{N_A}{1 + g_A\, e^{(E_A - E_F)/kT}}. \quad (4)$$

Here, p and n are free hole and electron concentrations, respectively. The degeneracy factors for donor and

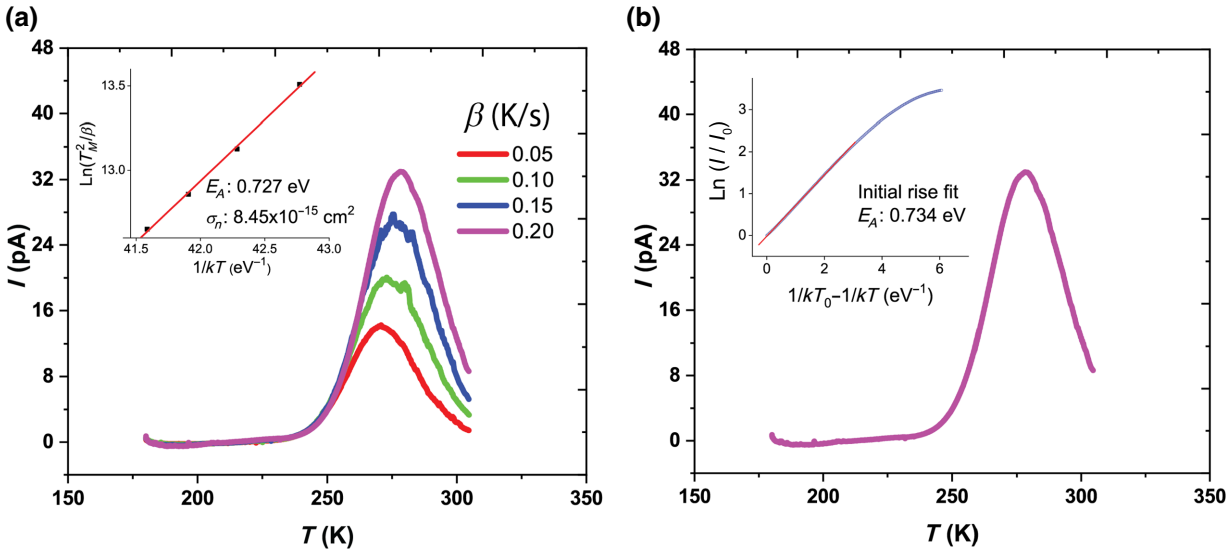

FIG. 3. (a) VHR TEES spectra and Arrhenius fit for the 280-K peak of O_2-annealed β-Ga_2O_3:Zr with an energy of 0.727 eV, and (b) energy estimated by initial rise method of about 0.734 eV.

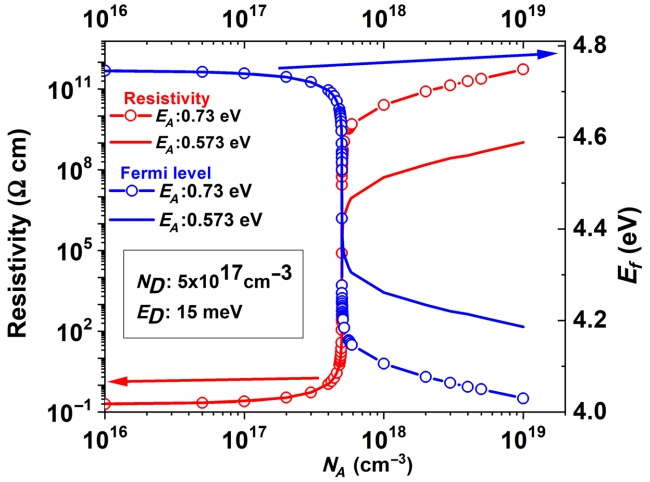

FIG. 4. Modeled Fermi-level position and resistivity in the O_2-annealed β-Ga_2O_3:Zr sample as a function of concentration of acceptors at 0.57 and 0.73 eV below conduction band.

acceptor levels are g_D and g_A, respectively, and E_F is the position of the Fermi level with reference to the valence-band edge.

Figure 4 shows the E_F positions and resistivity as the acceptor concentrations are varied over the range of 10^{16} to 10^{19} cm^{-3}. Clearly, the measured resistivity of about 7×10^{10} Ω cm is attained with the 0.73-eV trap, at concentrations of about 1×10^{18} cm^{-3} or higher, whereas the 0.57-eV trap is too shallow to pull the Fermi-level deep enough to cause the observed resistivity. The origin of the level at 0.573 eV cannot be identified from this study; however, levels with energies of 0.5–0.6 eV are reported to be likely associated with metallic impurities [24,40].

We next compare these defects in the annealed donor-doped sample with those measured on the unannealed acceptor-doped (Fe-na) sample. As shown in Fig. 5(a), two levels near about 275 and 320 K are prominent. The energy of the level near 275 K is estimated to be about 0.73 eV by the VHR method, indicating that the level is common to the Fe-doped and annealed Zr-doped samples. The dominant level near 320 K has an energy of (0.810 ± 0.028) eV, as shown in Fig. 5(b). Several studies report a level in the energy range of 0.7–0.8 eV. Our results indicate that there are, in fact, two closely spaced defects in this range. This is in agreement with Ingebrigtsen *et al.* [38], who report levels at 0.75 and 0.78 eV, with the former assigned to a native defect because of its appearance upon proton irradiation and the latter to a Fe acceptor. We assign the 0.81-eV level to Fe acceptors responsible for the high resistivity in the as-grown Fe-doped sample. On the other hand, the common level at about 0.73 eV in the O_2-annealed β-Ga_2O_3:Zr, sample and Fe-doped as-grown sample is likely associated with a native defect, which we further show below to be related to V_{Ga}.

B. Confirmation of the native defect identity by PAS

The type and concentration of open-volume defects is determined from PAS data. As noted earlier, Ga_2O_3 poses several challenges to PAS measurements. Determination of defect concentration, using Eq. (2), requires an S_b value for each of the crystallographic orientations. However, reliable determination of S_b for all orientations is missing due to the lack of measurements on high-quality defect-free Ga_2O_3 samples. Among the various samples characterized in our laboratory using PAS, the lowest S value is measured on an UID crystal grown by the CZ method using high-purity Ga_2O_3 source powder, referred to as HP. This lowest value of $S = 0.4160 \pm 0.0003$ is measured along the [001] direction and is used as S_b for estimating c_d. PAS data are presented in Fig. 6. The data presented in Fig. 6(a) display one type of annihilation at the surface (high S) and a single layer throughout the depth probed by the positron

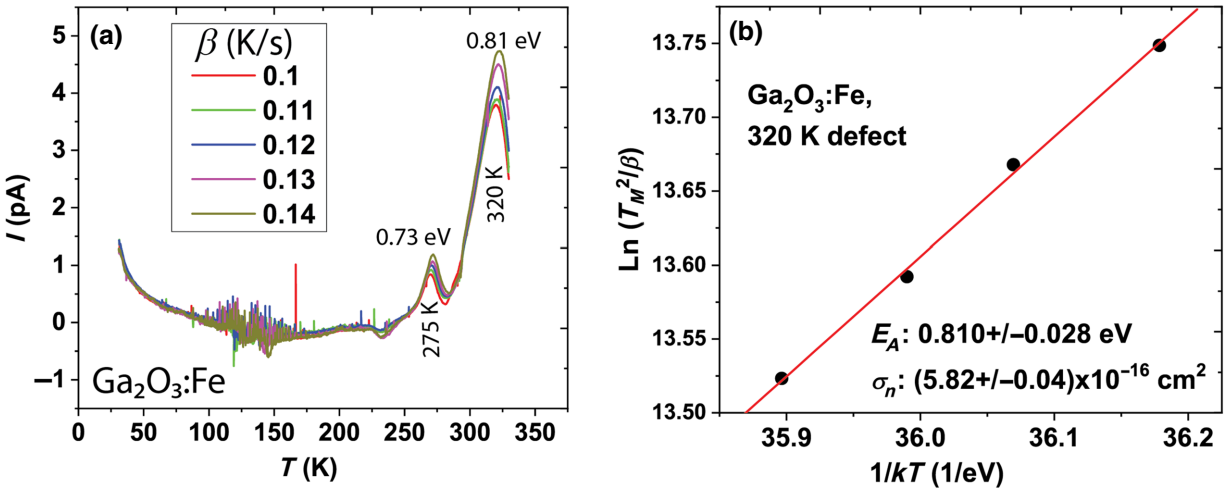

FIG. 5. (a) VHR TEES spectra for Fe-doped sample and (b) Arrhenius fit using Eq. (1) of the peak near 320 K.

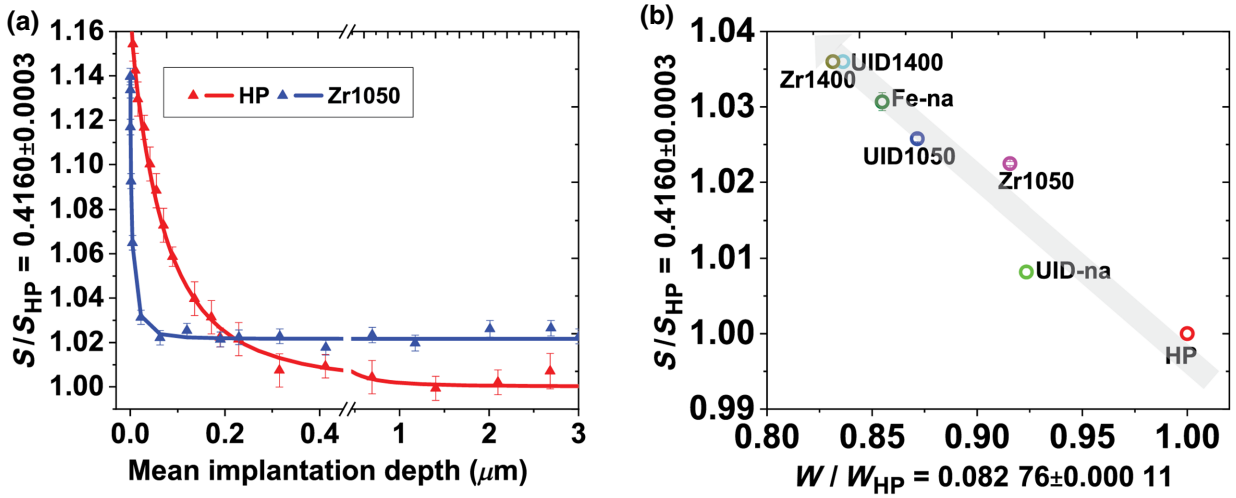

FIG. 6. (a) Depth profile of S parameter for HP and O_2-annealed Zr-doped samples, and (b) S vs W plot for HP and O_2-annealed Zr-doped, Fe-na, and UID samples with both as-grown and O_2-annealed conditions.

beam (approximately 6.3 μm). A custom fitting program, VEPFit[41], is applied to deconvolute the positron implantation profile from the diffusion length and provides S values for distinct layers of a damage depth profile [41]. Simple layers with constant annihilation characteristics are used. Fits are shown as solid lines in Fig. 6(a). The bulk S-W data are shown in Fig. 6(b). For clarity, only the HP sample and the Zr-doped sample annealed under O_2 at 1050 °C are shown in Fig. 6(a), whereas, in the S-W plot of Fig. 6(b), we also include the as-grown Fe-doped sample, an UID sample in the as-grown not-annealed state (UID-na) and following annealing in O_2 at 1050 or 1400 °C, and a Zr-doped sample annealed at 1400 °C. The resistivity in the UID samples is also observed to increase by various orders of magnitude, depending on annealing conditions.

Using the reported small dynamic range of <3% ($S_d \sim 1.03 \cdot S_b$) for Ga-vacancy defects in Ga_2O_3, and the measured bulk S value of the samples, which are found to be in the range from 2.25% above S_b to the upper end of the dynamic range, with respect to the HP sample, c_d is estimated to be in the range from about 1×10^{17} to 5×10^{18} cm^{-3} or higher.

We next estimate c_d from diffusion length L, which favorably shows less sensitivity to orientation and a larger dynamic range. The S parameter for the HP sample shows a gradual trend from annihilations at the surface (typically high S values) to a constant value of S deep in the sample (>1 μm), with a value of $S_b = 0.4160 \pm 0.0003$, which is the lowest among all samples. The L value for the HP sample is the longest measured at (92 ± 8) nm, which is close to what is expected in high-quality defect-free material, and is chosen as L_b in this study. The O_2-annealed sample shows a much more rapid initial decrease with implantation depth, and S levels off much closer to the surface to a constant value of S. The S value for all annealed samples is 2.25% to >3% above that for the HP sample, corresponding to short diffusion lengths between $L \sim 6$ and 10 nm.

It should be noted that a shorter diffusion length may also be interpreted as the presence of a positive potential at the surface that would repel positrons towards the bulk. Such a possibility is ruled out here. First, data shown in Fig. 6 indicate a significant increase in the S parameter after annealing, suggesting the presence of vacancies or their complexes or clusters that trap positrons. As the concentration of these defects increases, the diffusion length must decrease. The directly observed increase in S and the sharper transition with depth from the surface S value to the bulk S value, i.e., shorter diffusion length, both match our interpretation. Second, Lovejoy *et al.* discussed electric fields due to band bending in Ga_2O_3 and reported a potential caused by surface defects of only 0.5 V, positive at the surface, and extending to about 7 nm into the bulk [42]. Modeling PAS data with these parameters and a long diffusion length leads to poor fitting to the observed data. The shallow range of the electric field is incompatible with a long diffusion length and observed data.

Defect concentrations estimated using Eq. (3), using the diffusion length, fall in the range of (3–8) $\times 10^{18}$ cm^{-3} for all annealed samples, with approximately 20% uncertainty. The data trend for the Fe-doped sample has the second longest diffusion length, $L = (27 \pm 2)$ nm, which corresponds to $c_d \sim 3.8 \times 10^{17}$ cm^{-3}. However, the S value for this sample is the second highest. The discrepancy in the trend between L and S, as well as the small deviation from the straight line for some of the samples on the S-W plot, is likely the effect of orientation-dependent anisotropy.

Regarding the origin of the open-volume defect, we note from Fig. 6(b) that the bulk S and W values for all samples fall close to a straight line, suggesting one

type of open-volume defect in all samples. Under O_2-rich annealing conditions, the formation of gallium vacancies (or oxygen interstitials) is energetically favored, and an increased density of vacancies is observed by PAS on oxygen-annealed Si- and Sn-doped samples [43]. In addition, theoretical calculations indicate that oxygen vacancies are too small to trap positrons [44]. Therefore, the small observed change in the PAS signal is due to either a few large open-volume defects, such as V_{Ga}-V_O complexes or to high concentrations of smaller open-volume defects. The latter scenario is consistent with the model of resistivity based on the observed traps, estimated trap concentration, and short positron diffusion length.

The PAS results also support reported observations on Ga_2O_3. The range from defect-free S_b to the saturation value, S_d, is rather small, with 2–3% variation compared with a more common 4%–6% range in other materials, such as GaN and ZnO, an effect that is attributed to atypical relaxation of atoms near a gallium vacancy [35]. A near-neighboring Ga atom moves into the center of the vacancy, resulting in two smaller open volumes or split vacancies ($2V_{Ga}$-Ga_i), also designated as V^i_{Ga}; these structures are predicted by density-functional theory and observed by scanning transmission electron microscopy [45].

Hydrogen plays a major role in Ga_2O_3 and can occupy the open volume in the split Ga vacancy, since it is well documented to form O—H bonds and cannot exist in unrelaxed vacancies [17]. This would lower the positron Doppler signal S. Here, care is taken to avoid exposure to hydrogen during annealing and none is observed to be present through Fourier-transform infrared spectroscopy results for as-grown UID material. Furthermore, the introduction of hydrogen would be inconsistent with increasing resistivity, as it can passivate these acceptor states.

This indicates that the open-volume defect seen here is not likely to involve a neutral oxygen vacancy (V_O), dopants, hydrogen, or their complexes with V_{Ga}. The results strongly point towards split gallium vacancies as the defect identified by TEES at a depth of 0.73 eV ($E2^*$) below the conduction band that is responsible for the observed strong compensation of the shallow Zr donors after O_2 annealing.

IV. CONCLUSION

A defect level at about 0.73 eV ($E2^*$) with a concentration of about 10^{18} cm^{-3} is found to be responsible for more than 10 orders of magnitude increase in resistivity in O_2-annealed samples doped with shallow donors (Zr). Observations of a lower than typical range of variation in positron S parameter and the high concentration of open-volume defects estimated from the measured positron diffusion length support similar PAS observations and are consistent with a model of compensation based on split gallium vacancies. Careful positron measurements, as shown here, can quantify the concentration, in spite of the anisotropy of the S value, which depends on sample orientation with respect to incident positrons and collected annihilations. The positron diffusion length can be determined independently of the sample orientation and can provide more reliable information on open-volume vacancylike defect concentrations for Ga_2O_3 and other materials with similar challenges.

Data that support the findings of this study are available from the corresponding author upon reasonable request.

ACKNOWLEDGMENTS

This material is based upon work supported by the Air Force Office of Scientific Research under award No. FA9550-18-1-0507 (Program Manager: Dr. Ali Sayir). Any opinions, findings, and conclusions or recommendations expressed in this material are those of the authors and do not necessarily reflect the views of the U.S. Air Force. The authors thank Arkka Bhattacharya and Sriram Krishnamurty of University of Utah for making electrical contacts on some of the samples. We would also like to thank Professor Michael Scarpulla of University of Utah and John Blevins of the Air Force Research Laboratory for providing Fe-doped samples and powder for producing the HP crystal.

[1] S. I. Stepanov, V. I. Nikolaev, V. E. Bougrov, and A. E. Romanov, Gallium Oxide: Properties and applications - A review, Rev. Adv. Mater. Sci. **44**, 63 (2016).

[2] P. Jaiswal, U. Ul Muazzam, A. S. Pratiyush, N. Mohan, S. Raghavan, R. Muralidharan, S. A. Shivashankar, and D. N. Nath, Microwave irradiation-assisted deposition of Ga_2O_3 on III-nitrides for deep-UV opto-electronics, Appl. Phys. Lett. **112**, 021105 (2018).

[3] M. Higashiwaki, A. Kuramata, H. Murakami, and Y. Kumagai, State-of-the-Art technologies of gallium oxide power devices, J. Phys. D: Appl. Phys. **50**, 333002 (2017).

[4] Y. J. Wu, C. H. Hsieh, P. H. Chen, J. Y. Li, L. J. Chou, and L. J. Chen, Plasmon resonance spectroscopy of gold-in-gallium oxide peapod and core/shell nanowires, ACS Nano **4**, 1393 (2010).

[5] M. Higashiwaki, K. Sasaki, A. Kuramata, T. Masui, and S. Yamakoshi, Development of gallium oxide power devices, Phys. Status Solidi A **211**, 21 (2014).

[6] Z. Hu, K. Nomoto, W. Li, N. Tanen, K. Sasaki, A. Kuramata, T. Nakamura, D. Jena, and H. G. Xing, Enhancement-Mode Ga_2O_3 vertical transistors with breakdown voltage >1 KV, IEEE Electron Device Lett. **39**, 869 (2018).

[7] J. Xu, W. Zheng, and F. Huang, Gallium oxide solar-blind ultraviolet photodetectors: a review, J. Mater. Chem. C **7**, 8753 (2019).

[8] D. Agarwal, C. O. Aspetti, M. Cargnello, M. L. Ren, J. Yoo, C. B. Murray, and R. Agarwal, Engineering localized surface plasmon interactions in gold by silicon nanowire for

enhanced heating and photocatalysis, Nano Lett. **17**, 1839 (2017).

[9] M. J. Tadjer, J. L. Lyons, N. Nepal, J. A. Freitas, A. D. Koehler, and G. M. Foster, Editors' choice—review—theory and characterization of doping and defects in β-Ga_2O_3, ECS J. Solid State Sci. Technol. **8**, Q3187 (2019).

[10] A. T. Neal, S. Mou, S. Rafique, H. Zhao, E. Ahmadi, J. S. Speck, K. T. Stevens, J. D. Blevins, D. B. Thomson, N. Moser, K. D. Chabak, and G. H. Jessen, Donors and deep acceptors in β-Ga_2O_3, Appl. Phys. Lett. **113**, 062101 (2018).

[11] M. Saleh, A. Bhattacharyya, J. B. Varley, S. Swain, J. Jesenovec, S. Krishnamoorthy, and K. Lynn, Electrical and optical properties of Zr doped β-Ga_2O_3 single crystals, Appl. Phys. Express **12**, 085502 (2019).

[12] M. Saleh, J. B. Varley, J. Jesenovec, A. Bhattacharyya, S. Krishnamoorthy, S. Swain, and K. Lynn, Degenerate doping in β-Ga_2O_3 single crystals through Hf-doping, Semicond. Sci. Technol. **35**, 04LT01 (2020).

[13] P. Deák, Q. Duy Ho, F. Seemann, B. Aradi, M. Lorke, and T. Frauenheim, Choosing the correct hybrid for defect calculations: A case study on intrinsic carrier trapping in β-Ga_2O_3, Phys. Rev. B **95**, 075208 (2017).

[14] J. B. Varley, H. Peelaers, A. Janotti, and C. G. Van De Walle, Hydrogenated cation vacancies in semiconducting oxides, J. Phys. Condens. Matter **23**, 334212 (2011).

[15] C. Zimmermann, E. Frdestrom Verhoeven, Y. Kalmann Frodason, P. M. Weiser, J. B. Varley, and L. Vines, Formation and control of the E*2 center in implanted β-Ga_2O_3 by reverse-bias and zero-bias annealing, J. Phys. D: Appl. Phys. **53**, 9 (2020).

[16] B. E. Kananen, L. E. Halliburton, K. T. Stevens, G. K. Foundos, and N. C. Giles, Gallium vacancies in β-Ga_2O_3 crystals, Appl. Phys. Lett. **110**, 202104 (2017).

[17] P. Weiser, M. Stavola, W. B. Fowler, Y. Qin, and S. Pearton, Structure and vibrational properties of the dominant O-H center in β-Ga_2O_3, Appl. Phys. Lett. **112**, 232104 (2018).

[18] M. D. McCluskey, Point defects in Ga_2O_3, J. Appl. Phys. **127**, 101101 (2020).

[19] E. Korhonen, F. Tuomisto, D. Gogova, G. Wagner, M. Baldini, Z. Galazka, R. Schewski, and M. Albrecht, Electrical compensation by Ga vacancies in Ga_2O_3 thin films, Appl. Phys. Lett. **106**, 242103 (2015).

[20] P. Saadatkia, S. Agarwal, A. Hernandez, E. Reed, I. D. Brackenbury, C. L. Codding, M. O. Liedke, M. Butterling, A. Wagner, and F. A. Selim, Point and extended defects in heteroepitaxial β-Ga_2O_3 films, Phys. Rev. Mater. **4**, 104602 (2020).

[21] A. Y. Polyakov, N. B. Smirnov, I. V. Shchemerov, D. Gogova, S. A. Tarelkin, and S. J. Pearton, Compensation and persistent photocapacitance in homoepitaxial Sn-doped β-Ga_2O_3, J. Appl. Phys. **123**, 115702 (2018).

[22] M. M. Islam, N. Adhikari, A. Hernandez, A. Janover, S. Novak, S. Agarwal, C. L. Codding, M. Snure, M. Huang, and F. A. Selim, Direct measurement of the density and energy level of compensating acceptors and their impact on the conductivity of N-type Ga_2O_3 films, J. Appl. Phys. **127**, 145701 (2020).

[23] A. Y. Polyakov, N. B. Smirnov, I. V. Shchemerov, E. B. Yakimov, S. J. Pearton, C. Fares, J. Yang, F. Ren, J. Kim, P. B. Lagov, V. S. Stolbunov, and A. Kochkova, Defects responsible for charge carrier removal and correlation with deep level introduction in irradiated β-Ga_2O_3, Appl. Phys. Lett. **113**, 092102 (2018).

[24] K. Irmscher, Z. Galazka, M. Pietsch, R. Uecker, and R. Fornari, Electrical properties of β-Ga_2O_3 single crystals grown by the czochralski method, J. Appl. Phys. **110**, 063720 (2011).

[25] R. Sun, Y. K. Ooi, A. Bhattacharyya, M. Saleh, S. Krishnamoorthy, K. G. Lynn, and M. A. Scarpulla, Defect states and their electric field-enhanced electron thermal emission in heavily Zr-doped β -Ga_2O_3crystals, Appl. Phys. Lett. **117**, 212104 (2020).

[26] P. J. Schultz and K. G. Lynn, Interaction of positron beams with surfaces, thin films, and interfaces, Rev. Mod. Phys. **60**, 701 (1988).

[27] F. Tuomisto and I. Makkonen, Defect identification in semiconductors with positron annihilation: Experiment and theory, Rev. Mod. Phys. **85**, 1583 (2013).

[28] B. Šantić and U. V. Desnica, Thermoelectric effect spectroscopy of deep levels - application to semi-insulating GaAs, Appl. Phys. Lett. **56**, 2636 (1990).

[29] U. V. Desnica, M. Pavlović, Z. Q. Fang, and D. C. Look, Thermoelectric effect spectroscopy of deep levels in semi-insulating GaN, J. Appl. Phys. **92**, 4126 (2002).

[30] C. Szeles, Y. Shan, K. Lynn, A. Moodenbaugh, and E. Eissler, Trapping properties of cadmium vacancies ITe, Phys. Rev. B: Condens. Matter Mater. Phys. **55**, 6945 (1997).

[31] T. Ablekim, S. K. Swain, W. J. Yin, K. Zaunbrecher, J. Burst, T. M. Barnes, D. Kuciauskas, S. H. Wei, and K. G. Lynn, Self-Compensation in arsenic doping of CdTe, Sci. Rep. **7**, 1 (2017).

[32] K. H. Nicholas and J. Woods, The evaluation of electron trapping parameters from conductivity glow curves in cadmium sulphide, Br. J. Appl. Phys. **15**, 783 (1964).

[33] E. Korhonen, F. Tuomisto, O. Bierwagen, J. S. Speck, and Z. Galazka, Compensating vacancy defects in Sn- and Mg-doped In_2O_3, Phys. Rev. B: Condens. Matter Mater. Phys. **90**, 245307 (2014).

[34] W.-Y. Ting, A. H. Kitai, and P. Mascher, Crystallization phenomena in β-Ga_2O_3investigated by positron annihilation spectroscopy and X-ray diffraction analysis, Mater. Sci. Eng. B **91–92**, 541 (2002).

[35] A. Karjalainen, V. Prozheeva, K. Simula, I. Makkonen, V. Callewaert, J. B. Varley, and F. Tuomisto, Split Ga vacancies and the unusually strong anisotropy of positron annihilation spectra in β-Ga_2O_3, Phys. Rev. B **102**, 195207 (2020).

[36] J. B. Varley, H. Peelaers, A. Janotti, and C. G. V. d. Walle, Hydrogenated cation vacancies in semiconducting oxides, J. Phys. Condens. Matter **23**, 334212 (2011).

[37] A. Y. Polyakov, N. B. Smirnov, I. V. Shchemerov, S. J. Pearton, F. Ren, A. V. Chernykh, and A. I. Kochkova, Electrical properties of bulk semi-insulating β-Ga_2O_3 (Fe), Appl. Phys. Lett. **113**, 142102 (2018).

[38] M. E. Ingebrigtsen, J. B. Varley, A. Y. Kuznetsov, B. G. Svensson, G. Alfieri, A. Mihaila, U. Badstübner, and L. Vines, Iron and intrinsic deep level states in Ga_2O_3, Appl. Phys. Lett. **112**, 042104 (2018).

[39] Z. Zhang, E. Farzana, A. R. Arehart, and S. A. Ringel, Deep level defects throughout the bandgap of (010) β-Ga_2O_3 detected by optically and thermally stimulated defect spectroscopy, Appl. Phys. Lett. **108**, 052105 (2016).

[40] B. Wang, D. Look, and K. Leedy, Deep level defects in β-Ga_2O_3 pulsed laser deposited thin films and czochralski-grown bulk single crystals by thermally stimulated techniques, J. Appl. Phys. **125**, 105103 (2019).

[41] A. van Veen, H. Schut, M. Clement, J. M. M. de Nijs, A. Kruseman, and M. R. IJpma, VEPFIT applied to depth profiling problems, Appl. Surf. Sci. **85**, 216 (1995).

[42] T. C. Lovejoy, R. Chen, X. Zheng, E. G. Villora, K. Shimamura, H. Yoshikawa, Y. Yamashita, S. Ueda, K. Kobayashi, S. T. Dunham, F. S. Ohuchi, and M. A. Olmstead, Band bending and surface defects in β-Ga_2O_3, Appl. Phys. Lett. **100**, 181602 (2012).

[43] M. J. Tadjer, J. A. Freitas, J. C. Culbertson, M. H. Weber, E. R. Glaser, A. L. Mock, N. A. Mahadik, K. Schmieder, E. Jackson, J. C. Gallagher, B. N. Feigelson, and A. Kuramata, Structural and electronic properties of Si-And Sn-doped (-201) β-Ga_2O_3 annealed in nitrogen and oxygen atmospheres, J. Phys. D: Appl. Phys. **53**, 504002 (2020).

[44] I. Makkonen, E. Korhonen, V. Prozheeva, and F. Tuomisto, Identification of vacancy defect complexes in transparent semiconducting oxides ZnO, In_2O_3 and SnO_2, J. Phys. Condens. Matter **28**, 224002 (2016).

[45] J. M. Johnson, Z. Chen, J. B. Varley, C. M. Jackson, E. Farzana, Z. Zhang, A. R. Arehart, H. L. Huang, A. Genc, S. A. Ringel, C. G. Van De Walle, D. A. Muller, and J. Hwang, Unusual formation of point-defect complexes in the ultrawide-band-Gap semiconductor β-Ga_2O_3, Phys. Rev. X **9**, 041027 (2019).